INSTITUTE OF PHYSICS PUBLISHING PLASMA SOURCES SCIENCE AND TECHNOLOGY

Plasma Sources Sci. Technol. **13** (2004) 562–568 PII: S0963-0252(04)83492-3

Electron density measurements in afterglow of high power pulsed microwave discharge

M Mesko, Z Bonaventura, P Vasina, A Tálský, Z Frgala, V Kudrle and J Janča

Department of Physical Electronics, Masaryk University, Kotlarska 2, CZ-611 37 Brno, Czech Republic

E-mail: mesko@physics.muni.cz

Received 17 March 2004
Published 19 August 2004
Online at stacks.iop.org/PSST/13/562
doi:10.1088/0963-0252/13/4/002

Abstract

In this paper, we present experimental results of diagnostics of a high power microwave pulsed discharge (100 kW at 9 GHz, 2.5 μs) in nitrogen and oxygen gases. We used microwave interferometers operating at 15 and 35 GHz equipped with dielectric rod antennae. The operating pressure was between 20 and 2000 Pa. In nitrogen the large value of the recombination coefficient $\alpha_r = (1–2) \times 10^{-6}$ cm^3 s^{-1} suggests that N_2^+ ($\alpha_r = 2 \times 10^{-7}$ cm^3 s^{-1}) ions coexist with the predominant complex ions, N_4^+ and N_3^+, at pressures greater than 700 Pa. In oxygen the value of the recombination coefficient increases with increasing pressure from a value typical of O_2^+ ($\alpha_r = 3 \times 10^{-7}$ cm^3 s^{-1}) at a pressure of 200 Pa to a value of $\alpha_r = (2–4) \times 10^{-6}$ cm^3 s^{-1} at pressures above 1000 Pa as a consequence of the formation of O_4^+ at higher pressures.

1. Introduction

Pulsed discharges are often used in industrial plasmachemical processes, and their usage is growing. The main advantage of using pulsed discharges is the possibility of promoting complex chemical reactions without thermal loading of the substrate [1]. By varying the pulse length and its repetition rate, it is possible to choose the most favourable course of the reaction. Although there are many studies on the plasmachemistry of pulsed discharges, they have mostly used common supplies (dc, radiofrequency, microwave), with relatively low peak power (10^2–10^3 W). However, our work deals with pulse peak powers of the order of 10^5 W. Such a high power input during the pulse produces energetic electrons, highly excited species, metastables, radicals, etc, which can be advantageous for many plasmachemical applications.

When studying homogeneous plasmachemical reactions, heterogeneous (surface) reactions are often a complication. Therefore, we developed an experimental device in which the role of the plasma–wall reactions is suppressed. We achieved this by separating the plasma and the walls. In fact, the plasma was produced at the focal point of the microwave beam, which is 25 cm from the nearest wall. Therefore, diffusion to the walls was reduced.

Besides using electric probes, the microwave cavity method [2] is the most common technique for studying charged particle density. However, they both have certain limitations. Probe measurements are difficult to carry out in fast pulses and the resonator method is limited to plasmas with relatively small dimensions. Microwave interferometry can solve both these problems. It is based on measuring the phase shift of an electromagnetic wave passing through a plasma. Traditionally, spot-focused horn antennae have been used for coupling microwaves into a plasma. However, such an arrangement does not permit localized measurements. We employed movable dielectric rod antennae to overcome this limitation.

2. Theory

2.1. Method of measurement

Our method of determining the electron density as a function of time during the afterglow period consisted of measuring the time dependence of the phase change of an electromagnetic

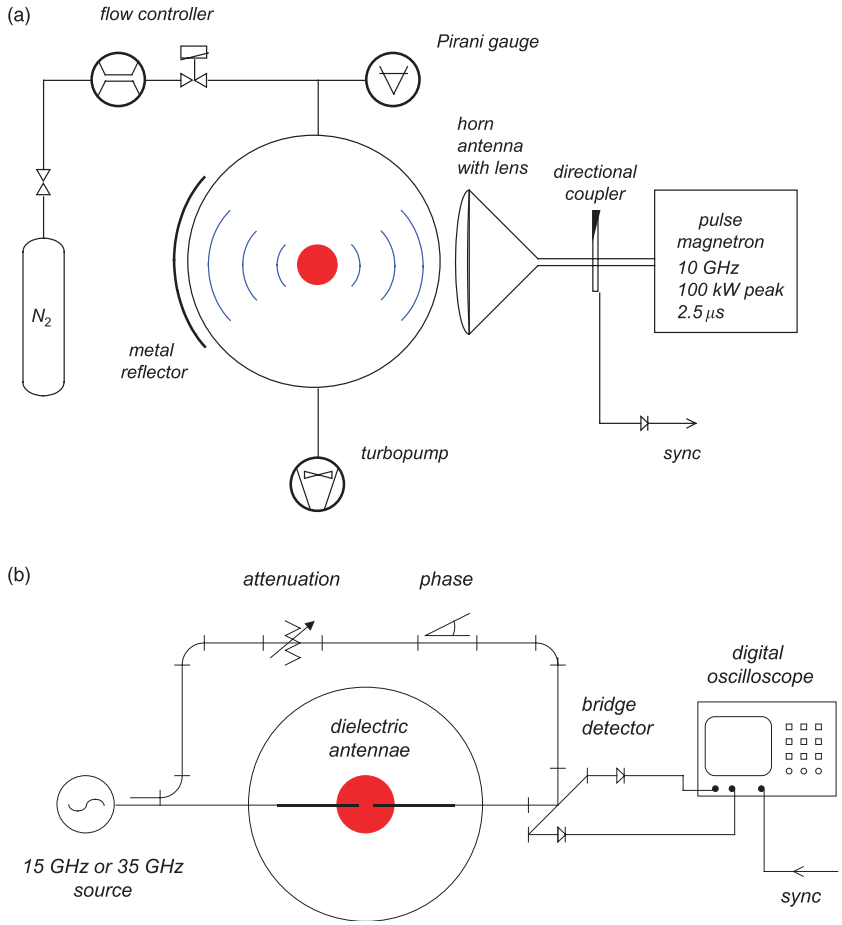

Figure 1. (*a*) Experimental set-up. (*b*) Microwave interferometer with dielectric rod antennae.

wave propagating through a plasma by means of microwave interferometry.

The complex dielectric permittivity of a plasma for a high frequency electric field has been shown [3] to be

$$\varepsilon_{\mathrm{p}} = 1 + \frac{ne^2}{\varepsilon_0 m\omega}\frac{4\pi}{3}\int_0^\infty \frac{1}{\omega - \mathrm{j}\nu_{\mathrm{m}}(v)}\frac{\mathrm{d}f_0(v)}{\mathrm{d}v}v^3\,\mathrm{d}v, \qquad (1)$$

where n, e and m are the electron density, charge and mass, respectively; ε_0 is the permittivity of vacuum; ν_{m} is the collision frequency for momentum transfer between electrons and gas particles; $f_0(v)$ is the steady-state isotropic part of the velocity distribution of electrons; and ω is the angular frequency of the electric field.

When a Maxwellian distribution is assumed and the collision frequency, ν_{m}, is independent of the electron velocity, v, this equation reduces to

$$\varepsilon_{\mathrm{p}} = 1 - \frac{ne^2}{\varepsilon_0 m\omega}\frac{\omega + \mathrm{j}\nu_{\mathrm{m}}}{\omega^2 + \nu_{\mathrm{m}}^2}. \qquad (2)$$

The phase shift is proportional to the difference between the propagation constants of the plasma and free space:

$$\Delta\phi = \mathrm{Im}\int_0^{L_{\mathrm{p}}} (\gamma_0 - \gamma_{\mathrm{p}})\,\mathrm{d}z. \qquad (3)$$

Using a first approximation of the propagation constant $\gamma = \mathrm{j}\varepsilon^{1/2}\omega/c$, considering a homogeneous medium and by substitution of equation (2) into equation (3), we obtain

$$\Delta\phi = \frac{ne^2}{2\varepsilon_0 mc}\frac{\omega}{\omega^2 + \nu_{\mathrm{m}}^2}L_{\mathrm{p}}. \qquad (4)$$

In the case of low pressures the collision frequency is much lower than the measuring frequency, $\nu_{\mathrm{m}}^2 \ll \omega^2$, and therefore it can be neglected in the denominator. The resulting relation for calculating the plasma density is

$$n = 4\pi\frac{\varepsilon_0 mc^2}{e^2}\frac{1}{L_{\mathrm{p}}\lambda_0}\Delta\phi. \qquad (5)$$

The electron density data have been obtained using the Mach–Zehnder configuration (as shown in figure 1(*b*)), which has an advantage in its simplicity of design and a high speed. The speed in following electron density changes is limited only by the response of the detector and the parasitic capacities and is in the range of tens of nanoseconds. The disadvantage is an ambiguity in phase shifts above 180° or 360°.

A pair of diode detectors are used on the E and H plane arms of a matched hybrid tee on a Mach–Zehnder interferometer as shown in figure 2. The field at the plasma arm output is $E_{\mathrm{p}} = E_{\mathrm{p0}}\cos(\omega t + \phi_{\mathrm{p}})$ and the field at the reference arm output is $E_{\mathrm{ref}} = E_{\mathrm{ref0}}\cos(\omega t + \phi_{\mathrm{ref}})$. Due to the properties of the hybrid tee, in one detector arm the signals are summed and in the other they are subtracted. Assuming a square law

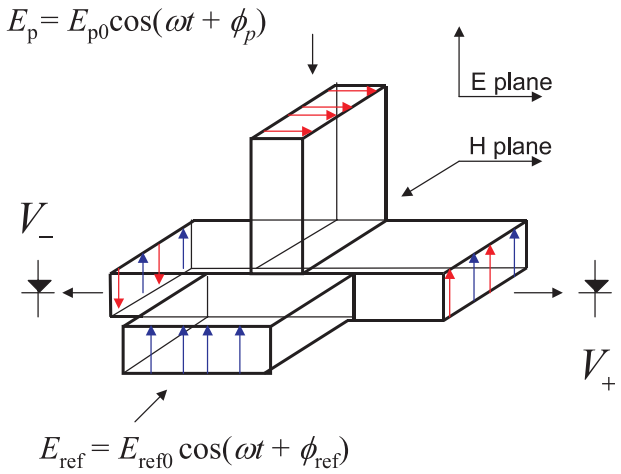

Figure 2. Schematic drawing of microwave fields in hybrid tee.

characteristic, the corresponding output voltages, V_+ and V_-, of the detectors are proportional to

$$V_\pm = k\frac{1}{4}\left(\frac{E_{p0}^2}{2} + \frac{E_{ref0}^2}{2} \pm E_{p0}E_{ref0}\cos(\phi_p - \phi_{ref})\right). \quad (6)$$

If both diodes are matched, we can calculate the sum and the difference of the detector voltages,

$$\begin{aligned} V_+ + V_- &= k\tfrac{1}{4}(E_{p0}^2 + E_{ref0}^2), \\ V_+ - V_- &= k\tfrac{1}{4}(2E_{p0}E_{ref0}\cos(\phi_p - \phi_{ref})). \end{aligned} \quad (7)$$

For the change of phase we can derive the formula

$$\cos^2(\phi_p - \phi_{ref}) = \frac{(V_+ - V_-)^2}{4(V_+ + V_-)|_{E_p=0}((V_+ + V_-) - (V_+ + V_-)|_{E_p=0})}. \quad (8)$$

By using the hybrid tee and a matched pair of diodes we are, therefore, able to calculate the phase shift from the measured data even when the amplitude of the signal in the plasma arm is changing. The value of $(V_+ + V_-)|_{E_p=0}$ is determined from a measurement with the probing arm fully attenuated. For maximum precision we also set the initial (without the plasma) value of phase difference $(\phi_p - \phi_{ref})$ to 90°.

From the signal difference between the detector output with the plasma on and with the plasma turned off, the phase difference was calculated. The plasma density was calculated consecutively using equation (5). It should be noted that this equation is valid only for low plasma densities, where the plasma frequency is much lower than the angular frequency $\omega_p \ll \omega$ [3].

2.2. Dielectric waveguide and dielectric rod antenna

In some applications dielectric waveguides and antennae are used instead of metallic ones. In a conductive waveguide the configuration of the electromagnetic field is given by transverse (most often TE) modes, but in a dielectric rod the field is more complicated and may be described by the so-called hybrid modes. The boundary condition is different, and so a small part of the electromagnetic field penetrates into the outer medium.

For good dielectrics, i.e. those with loss tangents of the order of 10^{-4}, the guided wavelength in an infinite medium is given by its permittivity, ε:

$$\lambda_g = \frac{\lambda_f}{\sqrt{\varepsilon}}, \quad (9)$$

where λ_f is the wavelength in free space.

When the medium is finite, the guided wavelength depends not only on the properties of the material but also on the dimensions. Also, the radiation pattern of a dielectric antennae depends on both the material and the size. For example, circular rod antennae with smaller diameters tend to lose more energy by radiation along the rod as the wave propagates. Because a substantial part of the energy propagates in the outer medium, the guided wavelength will be very close or equal to the outer medium (free space) wavelength, as opposed to the larger diameter ones, in which less energy radiates out and is rather reflected back into the antenna structure. As stated previously, this causes the guided wavelength to be shorter than the free space wavelength.

In contrast to the circular metal waveguides, matching the tangential components of the $\vec{E}$ and $\vec{H}$ fields at the interface requires a linear combination of the TE and TM modes. In a circular metal waveguide the situation is different because the boundary conditions ($E_z = 0$ and $E_\phi = 0$) can be satisfied for either the TE or TM mode. For a dielectric waveguide where the tangential components of the field are continuous at the boundary, in general neither the TE mode nor the TM mode alone can satisfy both E_z and E_ϕ being continuous and thus we must use a more general expression for the fields that are combinations of TE and TM modes. This is nothing more than stating that the general solution has both H_z and E_z components.

The components of the electric and magnetic fields for $r < a$ (inside the dielectric waveguide) for the HE mode are [4]

$$E_\phi = -\mathrm{j}\left[\frac{\alpha l}{r}A^e J_l(\Gamma r) - \omega\mu_0\Gamma A^m J_l'(\Gamma r)\right]\mathrm{e}^{-\mathrm{j}\alpha z}\cos(l\varphi), \quad (10)$$

$$E_z = (k_{ins}^2 - \alpha^2)A^e J_l(\Gamma r)\mathrm{e}^{-\mathrm{j}\alpha z}\sin(l\varphi), \quad (11)$$

$$H_\phi = \mathrm{j}\left[\frac{\alpha l}{r}A^m J_l(\Gamma r) - \omega\varepsilon\Gamma A^e J_l'(\Gamma r)\right]\mathrm{e}^{-\mathrm{j}\alpha z}\sin(l\varphi), \quad (12)$$

$$H_z = (k_{ins}^2 - \alpha^2)A^m J_l(\Gamma r)\mathrm{e}^{-\mathrm{j}\alpha z}\cos(\varphi l), \quad (13)$$

where

$$\Gamma = \sqrt{k_{ins}^2 - \alpha^2};$$

and for $r > a$ (outside the dielectric waveguide)

$$E_\phi = -\mathrm{j}\left[\frac{\alpha l}{r}B^e K_l(gr) - \omega\mu_0 g B^m K_l'(gr)\right]\mathrm{e}^{-\mathrm{j}\alpha z}\cos(l\varphi), \quad (14)$$

$$E_z = (k_{out}^2 - \alpha^2)B^e K_l(gr)\mathrm{e}^{-\mathrm{j}\alpha z}\sin(l\varphi), \quad (15)$$

$$H_\phi = \mathrm{j}\left[\frac{\alpha m}{r}B^m K_l(gr) - \omega\varepsilon_{out} g B^e K_l'(gr)\right]\mathrm{e}^{-\mathrm{j}\alpha z}\sin(l\varphi), \quad (16)$$

$$H_z = (k_{out}^2 - \alpha^2)B^m K_l(gr)\mathrm{e}^{-\mathrm{j}\alpha z}\cos(l\varphi), \quad (17)$$

where

$$g = \sqrt{\alpha^2 - k_{\text{out}}^2}.$$

Here α is the propagation constant in the z-direction, Γ is the transverse component in the dielectric waveguide, g is the transverse component outside the dielectric waveguide, J and K are Bessel and modified Bessel functions, and k_{ins} and k_{out} are wave vectors inside and outside the waveguide, respectively. The solution of this set of equations can be found, e.g. in [4].

We focus on the dominant mode in the circular dielectric waveguide. This dominant mode is called the HE_{11} mode. The HE_{11} mode has no cut-off frequency. The ratio of the phase velocity in a dielectric wire to the velocity in free space for this mode ($l = 1$) is given by

$$\frac{v_{\text{phase}}}{c} = \left(\frac{1}{x^2} + \frac{1}{y^2}\right)\left[\left(\frac{1}{x}\frac{J_1'(x)}{J_1(x)} + \frac{1}{y}\frac{K_1'(y)}{K_1(y)}\right) \times \left(\frac{\varepsilon_{\text{r-ins}}}{x}\frac{J_1'(x)}{J_1(x)} + \frac{\varepsilon_{\text{r-out}}}{y}\frac{K_1'(y)}{K_1(y)}\right)\right], \tag{18}$$

where x, y are

$$x = \Gamma\alpha \qquad y = g\alpha.$$

In figure 3 we show the ratios of the phase velocity in the dielectric wire to the velocity in the free space calculated from equation (18) for the dominant mode, HE_{11}, in the circular dielectric waveguide. The dotted curve refers to a dielectric wire with a relative permittivity of 2.1, whereas the corresponding solid curve refers to the same medium in the metal waveguide for the dominant TE_{11} mode. Both are plotted against the diameter of the guide measured in the free space wavelengths. For the larger diameters, the velocities in the dielectric waveguides and in the metal waveguides are substantially the same.

It means that by careful choice of the diameter of the dielectric rods it is possible to construct a microwave interferometer with the dielectric rod waveguides immersed in the plasma without perturbation of the propagating wave by the plasma. Only at the end of such a waveguide is the wave radiated out by the antenna and does it interact with the plasma, which makes the functioning of the interferometer possible. This configuration permits localized measurements where the microwaves are led by the dielectric waveguide through the plasma without any perturbation and the interaction zone is only the slab of plasma between the antennae.

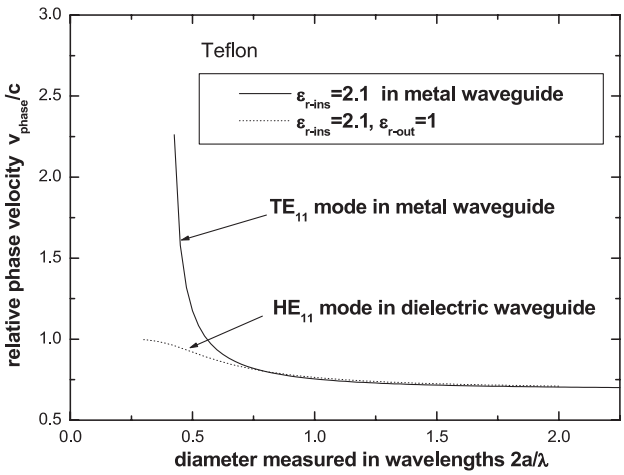

Figure 3. Relative phase velocity through a dielectric wire of relative permittivity 2.1 in free space and in the metal waveguide.

3. Experimental apparatus

3.1. Plasma generation

We have developed an apparatus (see figure 1(*a*)) where the volume processes are significant and the interaction of the plasma with the walls can be neglected. The plasma is produced in a spherical glass vessel with an inner diameter of 0.5 m. From one side the vessel is irradiated by a horn antenna. On the opposite side wall, an aluminium foil is placed to reflect and focus the microwaves. Microwaves (9 GHz, X-band) are generated by the pulse magnetron (the peak power reaches 100 kW). The pulses have 2.5 μs duration and are repeated 400 times per second. The electric field in front of the horn antenna is high enough (1 kV cm^{-1}) to produce a breakdown at reduced gas pressure. The field has a maximum in the centre of the glass vessel and therefore a plasma ball is formed there.

The experiment was carried out in a flow regime. The pressure was measured using a capacitance diaphragm gauge and maintained by a gas flow controller. The operating pressure was in the range 20–2000 Pa. Between measurements the system was pumped by a turbomolecular pump backed by a membrane pump down to a pressure of 10^{-4} Pa to suppress the role of the impurities in the nitrogen and oxygen afterglow.

Microwave interferometers operating at 15 and 35 GHz were used to measure the plasma density. They were coupled to the plasma by means of dielectric (PTFE) rod antennae. This configuration permits rather localized measurements, as the dielectric antennae were separated by 40 mm. The output signal from the interferometer was detected using diodes and then measured using an HP Infinium 500 MHz digital oscilloscope. The relatively large buffers of this device permitted us to record the data points with a time step of 10 ns. The synchronization pulses were taken from a -70 dB coupler.

3.2. Microwave interferometer with dielectric rod antennae

Figure 4 shows the calculated ratios of the phase velocity in the dielectric wire to the velocity in free space for the dominating mode, HE_{11}, in the circular dielectric waveguide. The curves refer to a dielectric wire of relative permittivity 2.1 (corresponding to Teflon) surrounded by a plasma of relative permittivity $\varepsilon_{\text{r-out}} = 0.95$, 0.75, 0.5 and 0.25. These values correspond to electron densities of 1×10^{11} cm^{-3}, 7×10^{11} cm^{-3}, 1×10^{12} cm^{-3} and 2×10^{12} cm^{-3}, respectively, for the 15 GHz measuring frequency and to electron densities 7×10^{11} cm^{-3}, 4×10^{12} cm^{-3}, 7×10^{12} cm^{-3} and 1×10^{13} cm^{-3}, respectively, for 35 GHz as given by $\varepsilon_{\text{r-out}} = 1 - n_e e^2/\varepsilon_0 \omega^2 m$. All values are plotted as a function of the diameter of the dielectric rod measured in free-space wavelengths.

For the larger diameters, the phase velocity of the wave is independent of the outside environment, and therefore the dielectric waveguide can be used for a transfer of the

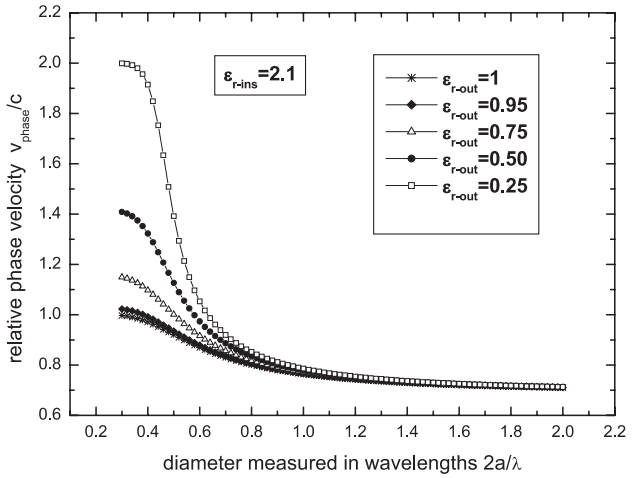

Figure 4. Relative phase velocity in a dielectric wire with a relative permittivity of 2.1 surrounded by plasma of various relative permittivities.

microwave signal in the probe arm of microwave interferometer even through the plasma with no perturbation of the phase due to the plasma.

The rod protrudes from the circular waveguide supporting the TE_{11} mode. This waveguide mode excites the hybrid mode, HE_{11}, on the rod. For 15 and 35 GHz bands we used rod diameters of 15 mm and 8 mm, respectively. In this case the waves are closely bound to the rod (see figure 4) and the outside plasma does not perturb the wave propagation in the rod. The antenna is $L = 9\lambda$ long, and it is tapered to a point at the end in order to achieve better matching [3] between the antenna and the plasma. We can use the approximation of a long rod [3], and the theoretical beam divergence is therefore

$$\theta \approx 60\sqrt{\frac{\lambda}{L}}\ (^\circ). \tag{19}$$

Our measured beam divergence is around 20°, which is in very good agreement with the theory.

4. Electron loss processes in the plasma volume

The variation of the electron density during the afterglow is, in general, the result of a number of competing processes. Let us consider a very simple model in which the plasma initially contains only neutral atoms, electrons and positive ions of one type. In addition, let the only significant electron removal processes be volume electron–ion recombination, electron attachment and ambipolar diffusion to the walls, where it is assumed that the charged particles are neutralized. In a spherical geometry the equation for charged particle decay by an electron–ion recombination, an electron attachment, and a diffusion followed by an efficient wall recombination can be written as

$$\frac{\partial n_{e,i}}{\partial t} = -\frac{D_a}{r^2}\frac{\partial}{\partial r}\left(\frac{r^2\partial n_{e,i}}{\partial r}\right) - \alpha_r n_e n_i - \nu_a n_e, \tag{20}$$

where n_e and n_i are the electron and ion densities, D_a is the ambipolar diffusion coefficient, α_r the recombination coefficient, ν_a is the attachment frequency and r is the radial position. Since the plasma is quasineutral, we have $n_e \cong n_i$, so that the second term on the right-hand side may be replaced by $(-\alpha_r n_e^2)$.

Table 1. Most significant nitrogen and oxygen ions responsible for recombinative electron losses in the afterglow.

Ion	Rate coefficient ($cm^3\ s^{-1}$)	Products	References
N_2^+	$1.8 \times 10^{-7}(300/T_e)^{0.39}$	$N(^4S)$	[5]
		$N(^2D)$	[6]
		$N(^3P)$	[7]
O_2^+	$2.7 \times 10^{-7}(300/T_e)^{0.7}$	$O(^3P)$	[5, 8]
	($T_e < 1200$ K)	$O(^1D)$	[9, 10]
	$1.6 \times 10^{-7}(300/T_e)^{0.55}$	$O(^1S)$	[11]
	($T_e > 1200$ K)		
N_3^+	$2 \times 10^{-7}(300/T_e)^{0.5}$	$N_2 + N$	[12]
N_4^+	$2 \times 10^{-6}(300/T_e)^{0.5}$	$N_2 + N_2$	[13, 14]
O_4^+	$2.3 \times 10^{-6}(300/T_e)^{0.5}$	$O_2 + O_2$	[15]

The plasma vessel is a sphere of radius $R = 25$ cm with corresponding characteristic diffusion length $\Lambda^2 = 64\,cm^2$. For this value of the diffusion length, the calculated loss volume processes predominate over the loss wall processes at all moderate pressures and electron densities. Thus the term for ambipolar diffusion to the walls in equation (20) can be neglected compared with the term for volume electron–ion recombination. In the case when the attachment can be neglected, too, the solution of equation (20) is given by

$$\frac{1}{n_e} = \frac{1}{n_e(0)} + \alpha_r t. \tag{21}$$

The curve representing the reciprocal of the electron density as a function of time during the afterglow period should be a straight line as long as the assumptions leading to equation (21) are valid. The slope of this line gives the value of the recombination coefficient.

If the attachment cannot be neglected (which is typical for the electronegative gases) the solution of equation (20) becomes

$$n_e = \frac{n_e(0)e^{-\nu_a t}}{1 + (\alpha_r n_e(0)/\nu_a)(1 - e^{-\nu_a t})}. \tag{22}$$

Again, by fitting the measured data by this function, the attachment and the recombination coefficients can be calculated.

The rate constants of significant electron–ion recombination processes are given in table 1.

The rate coefficient for attachment in oxygen according to [12] is

$$e + O_2 + O_2 \rightarrow O_2^- + O_2;$$

$$k_a = 1.4 \times 10^{-29}\left(\frac{300}{T_e}\right)\exp\left(-\frac{600}{T}\right) \times \exp\left(\frac{700(T_e - T)}{T_e T}\right)\ (cm^6\ s^{-1}), \tag{23}$$

where T and T_e are the gas temperature and electron temperature, respectively.

5. Experimental results

From equation (4) it follows that a lower operating frequency of the interferometer has an advantage—higher sensitivity. However, the phase shift can easily become greater than π,

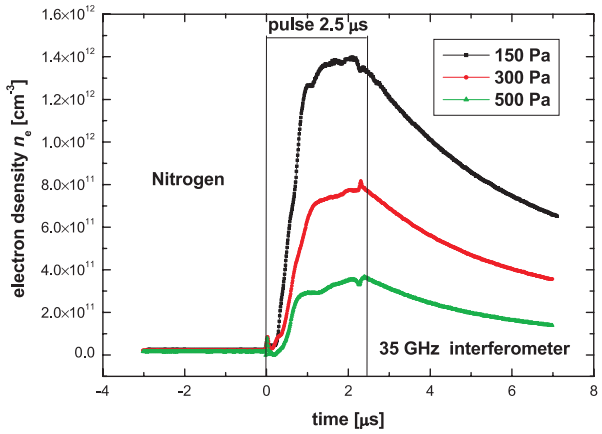

Figure 5. Time evolution of the electron density during the excitation pulse and in the early afterglow in nitrogen.

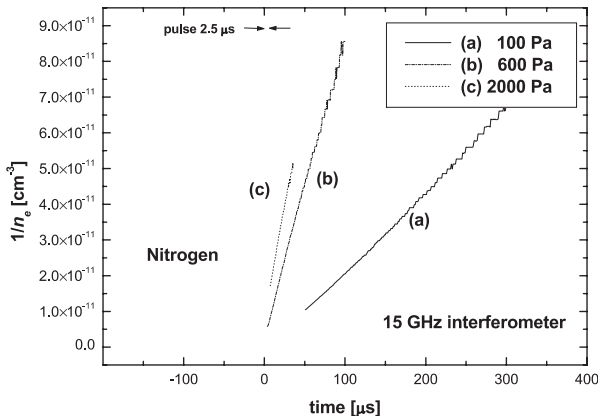

Figure 6. Reciprocal value of the electron density in the afterglow as a function of time in nitrogen at pressures (*a*) 100 Pa, (*b*) 600 Pa and (*c*) 2000 Pa, respectively.

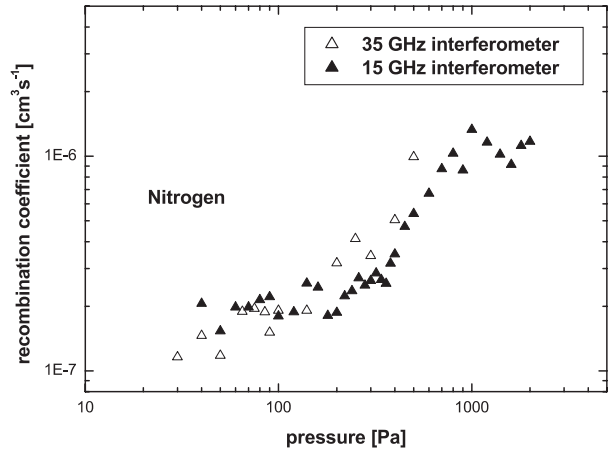

Figure 7. Recombination coefficient, α_r, in the nitrogen afterglow at various pressures.

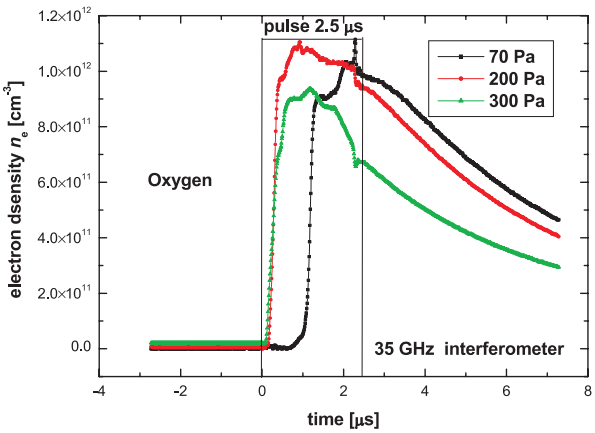

Figure 8. Time evolution of the electron density during the excitation pulse and in the early afterglow in oxygen.

and in such a way that it may introduce an ambiguity in evaluation of data. Therefore, we present the results of two interferometers with operating frequencies of 15 and 35 GHz.

5.1. Nitrogen afterglow

We measured the time evolution of the electron density in the pressure range 50–2000 Pa. Below 50 Pa, the microwave pulse does not ignite the nitrogen discharge. Examples of time evolution of the electron density in the nitrogen discharge at pressures of 150, 300 and 500 Pa are shown in figure 5.

In figures 6 curves (*a*)–(*c*) we show the electron density decay as a function of time in the nitrogen afterglow at pressures 100, 600 and 2000 Pa. The data are plotted as $1/n_e$ versus t to illustrate the linear dependence typical of recombination losses. In the early afterglow just after the end of the pulse the curve is not straight. In the later afterglow times the curves are very close to a straight line, which confirms that recombination is really the dominating loss process. The recombination coefficient remains at the value of 2×10^{-7} cm^3 s^{-1} in the pressure range 50–400 Pa. Then with increasing pressure the value of the recombination coefficient increases to a value of 1×10^{-6} cm^3 s^{-1} at 700 Pa and remains roughly at the same value up to 2000 Pa as shown in figure 7. The value 2×10^{-7} cm^3 s^{-1} at pressures below 400 Pa corresponds to the N_2^+ ion recombination coefficient. At pressures above 700 Pa, the N_2^+ ions convert into N_3^+ and N_4^+ ions by processes [12–14]. The values of the recombination coefficient $\approx 1 \times 10^{-6}$ cm^3 s^{-1} at pressures above 700 Pa correspond, then, to the N_3^+ and N_4^+ ion recombination coefficients.

5.2. Oxygen afterglow

In the case of oxygen gas, the microwave pulse does not ignite the oxygen discharge below a pressure of 70 Pa. Examples of the time evolution of the electron density in a oxygen discharge at pressures of 70, 200 and 300 Pa are shown in figure 8. As 70 Pa is the lower operational pressure limit in oxygen, there is an observable lag between plasma development and the rising edge of the microwave pulse.

Figures 9 curves (*a*)–(*c*) show the electron density decay as a function of time in the oxygen afterglow at pressures of 100, 600 and 1800 Pa. Again, the curves are close to a straight line and therefore recombination is the main loss process. Only for pressures higher than 1000 Pa is attachment observable as a small deviation from the straight line.

In figure 10 we present the recombination coefficient (calculated by fitting the data by equation (22)) as a function

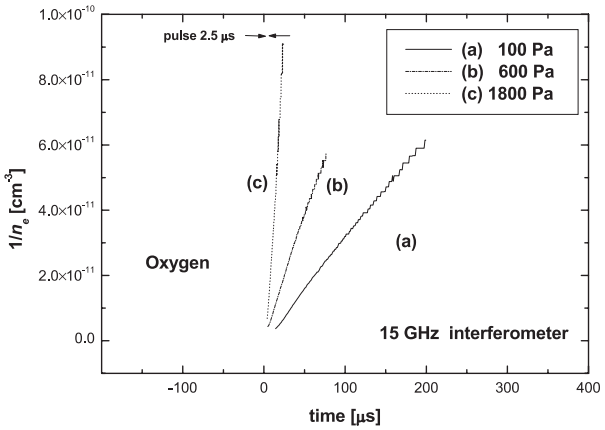

Figure 9. The electron density decay as a function of time in oxygen at pressures (*a*) 100 Pa, (*b*) 600 Pa and (*c*) 1800 Pa, respectively.

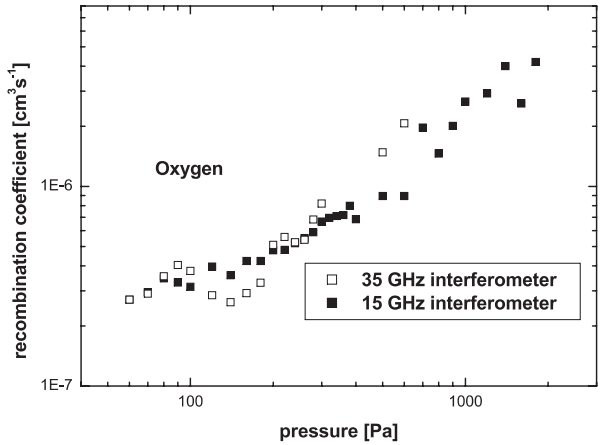

Figure 10. Recombination coefficient, α_r, in the oxygen afterglow at various pressures.

of the pressure. The situation is now different from the case of nitrogen afterglow discussed previously. The recombination coefficient, α_r, remains at the value of $3 \times 10^{-7}\,\mathrm{cm^3\,s^{-1}}$ in the pressure range 70–200 Pa. In oxygen gas the value of the recombination coefficient increases with pressure from a value of $3 \times 10^{-7}\,\mathrm{cm^3\,s^{-1}}$ at 200 Pa to the value $\alpha_r = (2\text{–}4) \times 10^{-6}\,\mathrm{cm^3\,s^{-1}}$ at pressures above 1000 Pa as the consequence of formation of O_4^+ at higher pressures [15].

In figure 11 the pressure dependence of the attachment frequency, ν_a (from the fit by equation (22)), and the corresponding electron temperature calculated from equation (23), are shown. The electron temperature seems to remain constant, around 2 eV.

6. Conclusion

A method that permits localized measurements of electron density by means of a microwave interferometer with dielectric waveguides terminating in tapered antennae has been developed. A dielectric waveguide of a sufficient diameter permits the guiding of microwaves through a plasma without phase shifts. The interaction zone is only the slab of plasma between the antennae.

We investigated the high power microwave pulsed discharge produced in the device with suppressed diffusion

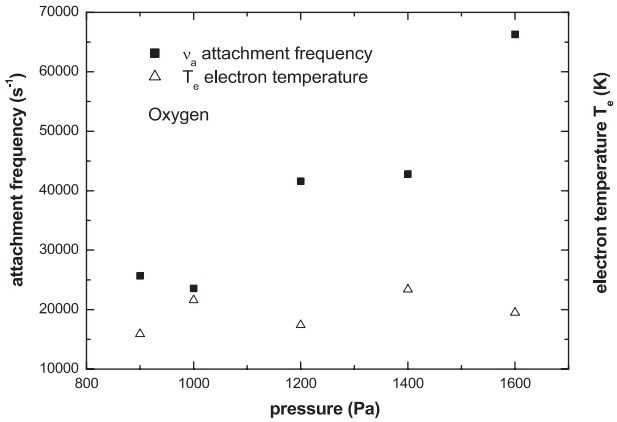

Figure 11. Pressure dependence of the attachment frequency and the corresponding electron temperature in oxygen.

losses by using a microwave interferometer operating at frequencies of 15 and 35 GHz. We observed that the dominant loss process was electron–ion recombination for both the gases studied, nitrogen and oxygen.

The measured recombination coefficients are very close to the results of other authors. It means that the conditions in the afterglow, especially the electron temperature, are not very different from the conditions in typical low power discharges.

Recombination coefficients for the higher pressures are influenced by the formation of N_3^+, N_4^+ and O_4^+ ions.

Acknowledgments

The skill of our technicians, P Saul and B Špaček, made the excellent performance of the vacuum system and the microwave interferometer possible. We are very grateful to Professor P Lukáč, from Comenius University of Bratislava, Slovakia, for valuable discussions.

This work was supported by projects GACR 202/01/P106, COST 527.20, MSM 143100003 and VEGA 1/0256/03.

References

[1] Lieberman M A and Lichtenberg A J 1994 *Principles of Plasma Discharges and Materials Processing* (New York: Wiley)
[2] Slater C J 1946 *Rev. Mod. Phys.* **18** 441
[3] Head M A and Wharton C B 1965 *Plasma Diagnostics with Microwaves* (New York: Wiley)
[4] Balanis C 1990 *Advanced Engineering Electromagnetics* (New York: Wiley)
[5] Mehr J F and Biondi A M 1969 *Phys. Rev.* **181** 264
[6] Frederick J E and Rush D W 1977 *J. Geophys. Res.* **82** 3509
[7] Zipf E C, Espy P J and Boyle C F 1980 *J. Geophys. Res.* **85** 687
[8] Walls F L and Dunn F H 1974 *J. Geophys. Res.* **79** 1911
[9] Torr D G *et al* 1979 *J. Geophys. Res.* **84** 3360
[10] Hays P B, Rusch D W, Roble R G and Walker J C G 1978 *Rev. Geophys. Space Phys.* **16** 225
[11] Zipf E C 1980 *J. Geophys. Res.* **85** 4232
[12] Kossyi I A, Kostinsky Yu A, Matveyev A A and Silakov V 1992 *Plasma Sources Sci. Technol.* **1** 207
[13] Fitaire M, Pointu A M and Stathopoulos D 1984 *J. Chem. Phys.* **81** 1753
[14] Monchy A R 1970 *A Study of the Nitrogen Afterglow* (Rotterdam: Drukkerij Bronder-Offset N.V.)
[15] Kasner H W and Biondi A M 1968 *Phys. Rev.* **174** 139